RAPID COMMUNICATION

Magnetic triangular bubble lattices in bismuth-doped yttrium iron garnet

Tao Lin(蔺涛)[1], Chengxiang Wang(王承祥)[1], Zhiyong Qiu(邱志勇)[2,3], Chao Chen(陈超)[1], Tao Xing(邢弢)[1], Lu Sun(孙璐)[4,5], Jianhui Liang(梁建辉)[4], Yizheng Wu(吴义政)[4], Zhong Shi(时钟)[6], and Na Lei(雷娜)[1,†]

[1] *Fert Beijing Institute, MIIT Key Laboratory of Spintronics, School of Integrated Circuit Science and Engineering, Beihang University, Beijing,* 100191, *China*

[2] *Key Laboratory of Materials Modification by Laser, Ion, and Electron Beams (Ministry of Education), School of Materials Science and Engineering, Dalian University of Technology, Dalian* 116024, *China*

[3] *Key Laboratory of Energy Materials and Devices (Liaoning Province), School of Materials Science and Engineering, Dalian University of Technology, Dalian* 116024, *China*

[4] *Department of Physics and State Key Laboratory of Surface Physics, Fudan University, Shanghai* 200433, *China*

[5] *School of Information Science and Technology, Shanghai Technology University, Shanghai* 201210, *China*

[6] *Shanghai Key Laboratory of Special Artificial Microstructure Materials and Technology & Pohl Institute of Solid State Physics, School of Physics Science and Engineering, Tongji University, Shanghai* 200092, *China*

(Received 14 October 2022; revised manuscript received 9 November 2022; accepted manuscript online 25 November 2022)

Magnetic bubbles have again become a subject of significant attention following the experimental observation of topologically nontrivial magnetic skyrmions. In recent work, tailoring the shape of the bubbles is considered a key factor for their dynamics in spintronic devices. In addition to the reported circular, elliptical, and square bubbles, here we observe triangular bubble domains in bismuth-doped yttrium iron garnet (Bi-YIG) using Kerr microscopy. The bubble domains evolve from discrete circular to latticed triangular and hexagonal shapes. Further, the orientation of the triangular bubbles in the hexagonal lattices can be flipped by decreasing the magnetic field. The sixfold in-plane magnetic anisotropy of Bi-YIG(111) crystal, which is presumably the mechanism underlying the triangular shape of the bubbles, is measured as 1179 erg/cm^3. The study of the morphologies of topologically trivial bubbles in YIG offers insight into nontrivial spin textures, which is appealing for future spintronic applications.

Keywords: magnetic bubble, yttrium iron garnet, Kerr microscopy, spintronics

PACS: 75.70.Kw, 75.30.Gw, 75.60.–d **DOI:** 10.1088/1674-1056/aca604

1. Introduction

Spin textures are ideal information carriers in spintronics-based devices. Magnetic bubbles are one of the most classical textures that have been studied intensely for non-volatile bubble memories for decades.[1–5] In recent years, progress has been made in skyrmion-based studies, which has led to magnetic bubbles regaining attention.[6–13] Both the magnetic textures form as a result of competition between magnetic energies, including magnetic exchange, anisotropy, demagnetization, and so on.[11,14] The spin textures can differ in topological charge, and in some cases, skyrmions can be equivalent to bubbles without Bloch lines at the domain wall.[12,15,16] In addition, in terms of dynamics, magnetic bubbles and skyrmions exhibit common features.[12] Thus, studies of magnetic bubbles may offer alternatives for understanding the physical features and benefit their future development in applications.

Very recently, the morphologies of skyrmions have attracted significant attention. Heart-shaped and polygonal magnetic skyrmions are proposed for improving the dynamic performances of skyrmion-based devices,[17,18] and elliptical skyrmions are experimentally realized in Pt/Co/Ta multilayers.[19] Moreover, skyrmion lattices with elliptical and square shapes are reported in bulk MnPtPdSn and GdRuSi magnets,[20–22] where their evolutions show similarities with the trivial bubbles reported in garnet materials.[23,24] Skyrmion bubbles have also been observed in thulium iron garnet (TmIG) based garnet materials,[25–28] indicating that the study of magnetic bubbles in YIG may offer alternatives for future skyrmion-based applications.

YIG takes advantage of the low damping and insulating character, and is therefore useful for spintronic applications.[29,30] In this work, we focus on the triangular bubbles observed in Bi-YIG material systems using magneto-optical Kerr microscopy. Bi-YIG is an outstanding magneto-optical material.[31,32] Therefore, we have selected Bi-YIG to study the magnetic structures using magneto-optical Kerr microscopy. We examine the evolution of magnetic textures, including circular, triangular, and hexagonal bubbles, and demonstrate that the orientation of the triangular bubbles can be flipped by changing the magnetic fields. Our work provides a prototype of bubble morphologies in garnets, which offers alternatives for spintronic applications.

[†]Corresponding author. E-mail: na.lei@buaa.edu.cn

© 2023 Chinese Physical Society and IOP Publishing Ltd

2. Experimental details

The single crystal Bi-YIG studied in this work was prepared using a liquid phase epitaxy (LPE) technique on (111) orientated gadolinium gallium garnet (GGG) substrate. Additional Bi_2O_3 was added in normal PbO–B_2O_3–Fe_2O_3–Y_2O_3 flux to dope bismuth into YIG. The ratio of bismuth to yttrium in the Bi-YIG was approximately 1:5, and the thickness was fixed at approximately 3 μm. To measure the magnetic hysteresis loops of the samples, magneto-optical Kerr effect (MOKE) measurements with longitudinal and polar configurations were taken. Rotating-of-field MOKE (Rot-MOKE) evaluation was performed to analyze the magnetic anisotropy for the YIG sample.[33–35] The applied field sweeped polar angles where the magnetic anisotropy between in-plane and out-of-plane directions can be evaluated. To observe magnetic textures in the Bi-YIG sample, a commercial Kerr microscope and electromagnets (Evico Magnetics) were used. In the observation, a polar sensitivity setup with out-of-plane magnetic fields was applied. Fast Fourier transform (FFT) was applied to the Kerr microscopy images to analyze the symmetry of the bubble lattices. To examine the underlying physics of the bubble domain morphologies in the Bi-YIG sample, vector vibrating sample magnetometer (VSM) measurement was conducted to evaluate the in-plane magnetic anisotropy.[36] Note that, unlike the Rot-MOKE measurement, the anisotropy measured by vector VSM is in-plane, where the applied field rotating angles are azimuthal.

3. Results and discussion

3.1. Magnetic properties of the samples

The magnetic hysteresis loops of the sample are shown in Fig. 1(a). The magnetic easy axis of the sample is in-plane, as seen from the red loops. A zoomed-in image of the in-plane loop is shown as an inset, where the coercive field and saturation field are 18 Oe and 50 Oe, respectively. The out-of-plane hysteresis loop (the blue curve) shows almost zero remanence magnetization and higher saturation field of $H_S = 1800$ Oe, which is the typical anisotropy field of the YIG film.

Figure 1(b) shows the results of the Rot-MOKE measurement. The rotating magnetic field applied to the Bi-YIG samples is set to 3000 Oe, which is far above the saturation field H_S even along the hard axis. Due to the competition between the magnetic anisotropy and applied fields, the magnetic moments align in equilibrium orientation, as illustrated in the inset. When the applied field rotates, orientation deviation occurs between the magnetization and the applied field. In addition, the energy density of unit volume in this case can be written as[34,35,37]

$$E = -M_s H\cos(\alpha-\theta) + K_u\sin^2(\theta) + K_4\sin^2\left(\theta+\frac{\pi}{4}\right)\cos^2\left(\theta+\frac{\pi}{4}\right), \quad (1)$$

where M_s is the saturation magnetization, H is the applied field, K_u is the uniaxial anisotropy constant, and K_4 is the fourfold anisotropy constant. The angles of the applied field and magnetic moment correlating with the easy axis (in-plane direction x) are defined as α and θ, as seen in the inset of Fig. 1(b).

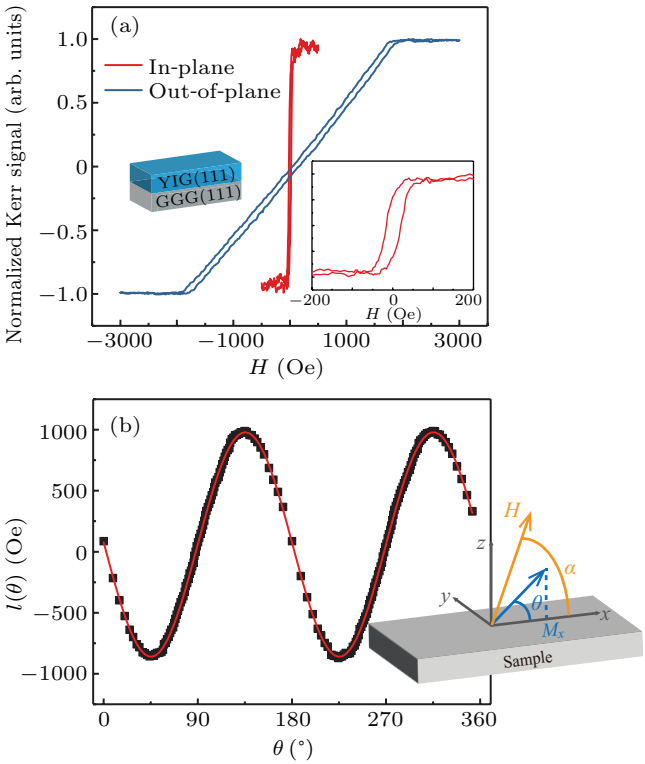


Fig. 1. (a) In-plane and out-of-plane magnetic hysteresis loops of the YIG sample. The figure presents a schematic drawing of the sample structure. A zoomed-in image of the in-plane loop is shown as an inset. (b) The magnetic torque $l(\theta)$ as a function of the angle of the in-plane magnetic field. The red line indicates the fitting for the torque. Inset: illustration of the magnetic field and magnetization directions in the Rot-MOKE measurement.

Through minimizing the magnetic energy density E, the torque $l(\theta)$ on magnetization can be obtained from Eq. (1) as[34,35,37]

$$\begin{aligned} l(\theta) &= H\sin(\alpha-\theta) \\ &= \frac{1}{2}H_{ku}\sin 2(\theta-\theta_u) - \frac{1}{4}H_{k4}\sin(4\theta), \end{aligned} \quad (2)$$

where θ_u is the easy axis angle correlated with the x axis, and H_{ku} and H_{k4} are the uniaxial and fourfold anisotropy fields, respectively. Based on Eq. (2) with free parameter fitting, H_{ku} is −1839 Oe, H_{k4} is 18 Oe, and θ_u is 0.3°. The fitting curve is shown in red in Fig. 1(b). It is clear that the fourfold anisotropy field H_{k4} is relatively small. This result is not considered in the following discussion. The value of the uniaxial anisotropy field H_{ku} is consistent with the saturation field in the hard axis loop shown in Fig. 1(a). The negative H_{ku} represents an in-plane magnetic easy axis, which aligns with the

hysteresis loop measurements. The small θ_u of 0.3° indicates precise control of the angles of the sample and magnetic field in the measurements. Taking the saturation magnetization as 139 emu/cm^3 into $H_{ku} = 2K_u/M_s$,[38] the uniaxial anisotropy constant K_u is approximately -1.28×10^5 erg/cm^3.

3.2. Evolution of magnetic structures under out-of-plane magnetic fields

The results of the Kerr microscopy observation of the magnetic textures in the Bi-YIG samples are presented in Fig. 2. Note that the same area of the sample is observed continuously by sweeping the out-of-plane magnetic field H_z. Before varying the fields, a background image is taken when the sample is in the positive saturation state at $H_z = 3000$ Oe. Subsequently, the applied magnetic field is swept, each image is recorded and subtracted by the saturation background, and the contrast of the magnetic structure is shown in Fig. 2. In addition to the Kerr microscopy images, FFT is applied to each image to check the asymmetries of the magnetic patterns.

When the applied perpendicular field decreases from saturation, isolated magnetic bubbles start to nucleate ($H_z =$ 1810 Oe). Since the bubble density is low, no obvious symmetrical information can be distinguished in the FFT result, as shown by the insets in the upper-right corner. Then, the bubble density continues to increase, a hexagonal symmetry gradually occurs ($H_z = 1633$ Oe and 1457 Oe). The hexagonal symmetry of the magnetic bubbles is clearer when $H_z = 1291$ Oe is applied. Considering the results of the magnetic anisotropy evaluation in this work, the generation of magnetic bubbles should be a result of competition between the applied magnetic field and magnetic anisotropic energies, such as crystal and shape anisotropies.

From saturation to the formation of a magnetic bubble lattice, the density and size of the bubbles gradually increase. The number of bubbles reaches its maximum when the hexagonal bubble lattice is well formed. With further decrease of the magnetic field, the bubbles expand in size, and some of them deform into stripe domains to compensate for the reduction of Zeeman energy. The generation of stripe domains obscures the hexagonal symmetry in the FFT image. In the whole process of sweeping magnetic fields, the magnetic bubbles remain several microns in size, despite their expansion with fields.

Another interesting observation is that at a certain range of magnetic fields, the magnetic bubbles do not present circular shapes. For example, when $H_z = 1291$ Oe, the bubbles are triangular, and they are hexagonal when $H_z = 48$ Oe. The triangular bubble shape in garnet was reported decades ago,[24] but its transformation under magnetic fields was not investigated. Because the morphology of spin textures is important in spintronic applications, we further increase the magnification of the Kerr microscopy imaging to study the morphologies of the bubbles with respect to magnetic fields.

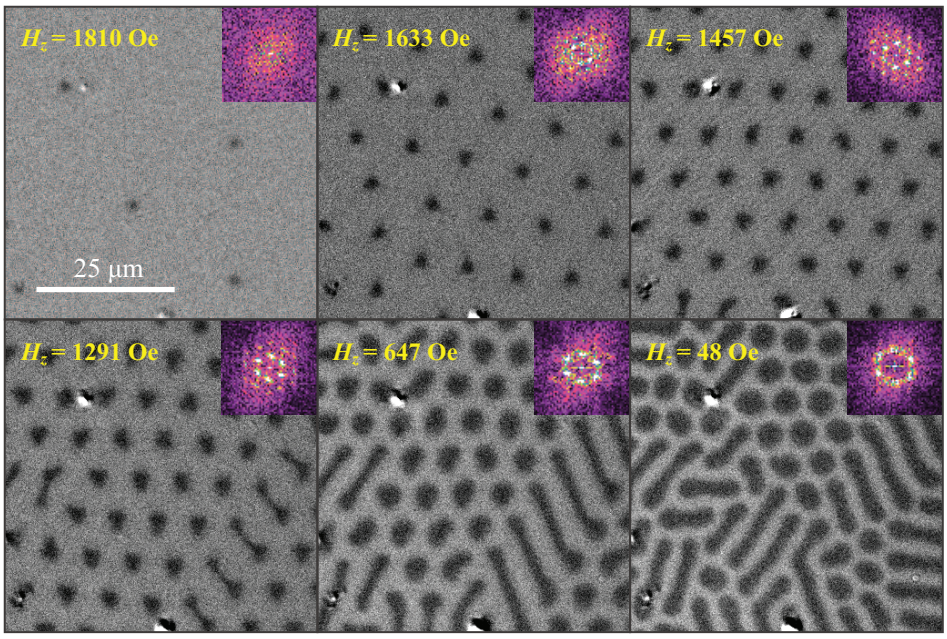


Fig. 2. Magnetic structures of the Bi-YIG sample when applying various out-of-plane magnetic fields H_z (indicated in each image). FFT results are shown as insets in the top-right corner of each image.

3.3. Magnetic bubble morphologies

We further observed the shapes of the magnetic bubbles at higher magnifications. A fixed area of the sample was subjected to Kerr microscopy imaging with varying H_z. The results are shown in Fig. 3. At $H_z = 1681$ Oe, the bubbles are nucleated, and the magnetic bubbles are circular in shape, as illustrated by the white circles in the images. At $H_z = 246$ Oe, the magnetization is near the remanence state; the magnetic bubbles tend to transform into stripe domains, and the bubbles

present a hexagonal shape. However, when the bubbles are in lattice states ($H_z = 1340$ Oe, 1291 Oe, and 1242 Oe), they are clearly triangular in the highly magnified view. The triangle overlays are provided to show the shape and orientation of the triangular bubbles and make it possible to investigate the evolution of the magnetic bubbles when varying the magnetic field H_z.

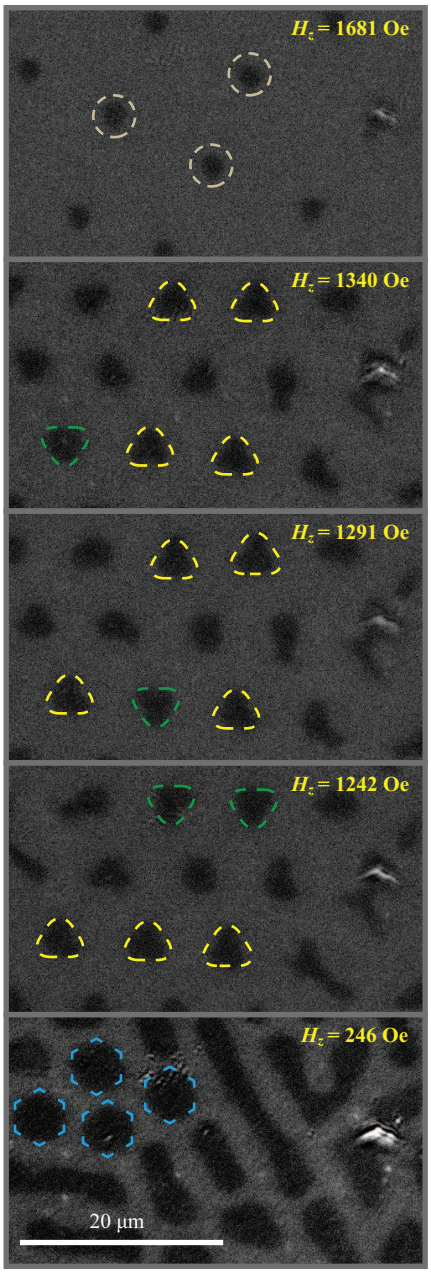


Fig. 3. Field-dependent morphologies of the magnetic bubbles. The applied out-of-plane magnetic fields H_z are indicated in each image. Dashed line frames with different shapes and colors are shown to illustrate the bubble morphologies.

Interestingly, we find that the direction to which the bubbles point can be changed by changing the out-of-plane magnetic field. For example, when H_z decreases from 1340 Oe to 1291 Oe, a magnetic bubble in the yellow frame flips from pointing up to pointing down, while the bubble in the green frame flips in the opposite direction. Then, when H_z reaches 1242 Oe, the flip of bubbles happens again. In this process, it seems that the bubbles can flip randomly once or twice, although some bubbles do not flip.

For topologically nontrivial skyrmions, the Dzyaloshinskii–Moriya interaction (DMI) and magnetic anisotropy in the materials determine the size, shape, and stabilization of the magnetic structures, which, according to recent studies on the morphologies of skyrmions, are not circular.[17–20] For instance, it is shown that in Pt/Co/Ta multilayers, anisotropic DMI and in-plane anisotropy deform magnetic skyrmions to elliptical shapes.[19] Although bismuth is a remarkable material with strong spin–orbit coupling,[39] the DMI is considered weak in our Bi-YIG sample. The lattice structure of YIG is centrosymmetric, where bulk DMI is not significant. Our Bi-YIG has a thickness in micrometers, and the interfacial DMI should also be negligible. In addition, it is reported that no DMI is shown in GSGG/Bi-YIG/Pt material structure.[40] Therefore, except for DMI, we assume that the generation of triangular bubbles could be attributed to the sixfold in-plane magnetic anisotropy.

To study the in-plane magnetic anisotropy, vector VSM measurement was conducted.[36] An illustration of the measurement is shown in Fig. 4(a). A constant in-plane field (H_i) of 50 Oe is applied to saturate the magnetization and is rotated in the sample film plane to drive the moments. Magnetization parallel/perpendicular to the applied in-plane field (m_x/m_y) is measured simultaneously. As a result of the in-plane anisotropy, the magnetization cannot remain parallel to the applied field. Since the angle between the applied field and the starting direction (φ_H) is known, the angle between the magnetization and the starting direction (φ_m) can be calculated as $\varphi_m = \varphi_H - \arctan(m_y/m_x)$. Further, the magnetic torque l_i can be calculated as $l_\mathrm{i} = m \times H_\mathrm{i}/V \approx m_y H_\mathrm{i}/V$, where m is the magnetization and V is the volume of the magnetic layer. l_i versus φ_m is shown in Fig. 4(b), where the trend of the data is significantly different from that observed for the uniaxial and fourfold anisotropies. Considering the sixfold in-plane anisotropy, we fit the l_i according to[36,41]

$$l_\mathrm{i} = K_\mathrm{iu} \sin 2(\varphi_m - \varphi_2) - \frac{1}{2} K_\mathrm{i4} \sin 4(\varphi_m - \varphi_4) - \frac{1}{18} K_\mathrm{i6} \sin 6(\varphi_m - \varphi_6), \quad (3)$$

where K_iu, K_i4, and K_i6 represent the uniaxial, fourfold, and sixfold in-plane anisotropies, respectively, and φ_2, φ_4, and φ_6 are easy axis angles related to the starting direction of the rotating fields. A well-fitting result is shown in Fig. 4(b), and the absolute values of K_iu, K_i4, and K_i6 are approximately 395 erg/cm^3, 138 erg/cm^3, and 1179 erg/cm^3, respectively. Therefore, through the dominance of K_i6, we confirm the sixfold in-plane anisotropy in the Bi-YIG sample. The magnetic bubbles result from the competition of energies, including anisotropy energies in different directions. It has been

shown that in-plane magnetic anisotropy can induce the elliptical deformation of magnetic skyrmions.[19] In our Bi-YIG, the sixfold in-plane magnetic anisotropy can induce triangular and hexagonal bubble morphologies. At low magnetic fields, the bubbles are hexagonal, and the sixfold in-plane anisotropy may be the primary cause of this morphology. For the triangular bubbles, it is shown that their orientation can be flipped randomly by varying the magnetic field in the experiment observation. In the presence of sixfold in-plane magnetic anisotropy, anisotropic energies can be equivalent for the bubbles in two orientations. With disturbance, the bubbles may flip randomly. Besides the sixfold in-plane anisotropy, other underlying physics might contribute to the formation of the bubble morphologies. This possibility requires further study. The analysis of the relation between in-plane anisotropy and bubble shape could offer alternatives to potential morphology-based manipulation methods in spintronic applications in garnets.

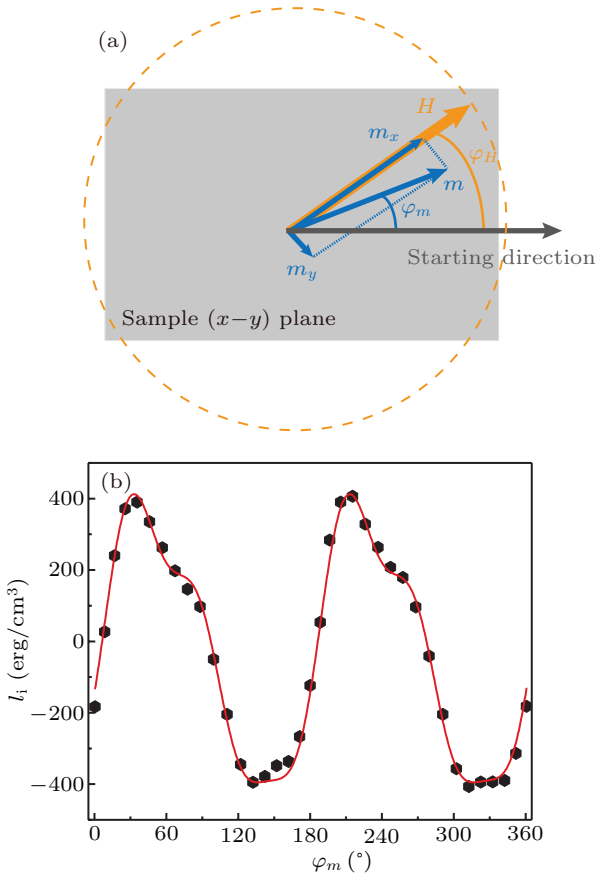


Fig. 4. (a) Illustration of field and magnetization directions in the vector VSM anisotropy measurement. (b) Solid points: the magnetic torque l_i versus φ_m. The red line indicates the fitting for the torque.

Based on the high-magnification view of the magnetic structures, the statics of the magnetic bubbles are analyzed, as shown in Fig. 5. A fixed view of 55×42 μm^2 is observed with various perpendicular fields H_z. Since the bubbles take different shapes with the transformation of the domain structures, the evaluation of the bubble diameters is not sufficiently meaningful for the bubble size. Therefore, the area of a single bubble under H_z is analyzed, as shown in the upper panel in Fig. 5. In addition to the bubble size, the distances between two neighboring bubbles are measured. The borders of bubbles are first selected in order to determine their centers. The distances, as shown in the bottom panel in Fig. 5, are measured between the centers of two neighboring bubbles. The external field decreases from saturation to near zero. Hence, the evolution of the magnetic structures is similar to that in Fig. 2, and the dominant magnetic texture changes with various H_z. When H_z decreases from saturation, isolated bubbles gradually nucleate and expand, causing drastic change in the distance between bubbles. Then, triangular bubbles arrange in a hexagonal lattice form. In this case, the area of a single bubble continues to increase as a result of the continuously changing Zeeman energy. However, the distance between bubble centers remains almost unchanged, indicating that the bubble lattice structure is stable. When H_z is small, large hexagonal bubbles and stripe domains are shown, and the sizes of and distances between bubbles continue to change due to the deformation of the bubble lattices and external fields.

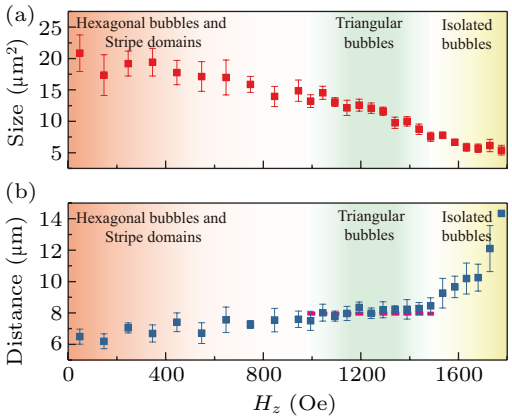


Fig. 5. Statistics for the magnetic structures in the YIG sample with varying H_z. (a) Area of single bubble. (b) Distance between bubbles. Colored parts indicate the dominant magnetic structures in the observed area: hexagonal bubbles and stripe domains (orange), triangular bubbles (green), and isolated bubbles (yellow). A dashed line is included in the lower scheme of the figure to clarify the distances between the triangular bubbles arranged in a hexagonal lattice.

4. Conclusion

In this work, we experimentally realize magnetic bubble lattices in Bi-YIG/GGG (111) samples. Magnetic structures are observed using Kerr microscopy. The evolution of magnetic textures in the Bi-YIG samples under varying perpendicular magnetic fields is investigated. Using the FFT of the imaging results, the symmetries of the spin textures are evaluated and three different phases of the bubbles are defined. Magnetic properties such as hysteresis loops and anisotropies are measured. These properties may explain the phenomena observed in this work. For the magnetic bubble lattice phase, triangular bubbles are found. In addition, the orientation of the triangular bubbles can be changed by changing the magnetic

field, which may offer an opportunity to manipulate and utilize spin textures. Since the morphologies of skyrmions have potential for applications and magnetic bubbles are closely related to topologically nontrivial magnetic skyrmions, this work provides alternatives to skyrmions and bubbles in magnetic garnets, which may be feasible for spintronics based devices and logics.

Acknowledgements

N. L. acknowledges support by the National Natural Science Foundation of China (Grant Nos. 52061135105 and 12074025). Y. W. acknowledges support by the National Natural Science Foundation of China (Grant Nos. 11974079, 12274083, and 12221004), and the Shanghai Municipal Science and Technology Basic Research Project (Grant No. 22JC1400200).

References

[1] Suzuki R 1986 *Proc. IEEE* **74** 1582
[2] Bonyhard P, Geusic J, Bobeck A, Yu-Ssu C, Michaelis P and Smith J 1973 *IEEE Trans. Magn.* **9** 433
[3] Huang M and Zhang S 2002 *Mater. Chem. Phys.* **73** 314
[4] Mallmann E J J, Sombra A S B, Goes J C and Fechine P B A 2013 *Solid State Phenom.* **202** 65
[5] Fechine P B A, Silva E N, de Menezes A S, Derov J, Stewart J W, Drehman A J, Vasconcelos I F, Ayala A P, Cardoso L P and Sombra A S B 2009 *J. Phys. Chem. Solids* **70** 202
[6] Fert A, Reyren N and Cros V 2017 *Nat. Rev. Mater.* **2** 17031
[7] Du H and Wang X 2022 *Chin. Phys. B* **31** 087507
[8] Tang J, Kong L, Wang W, Du H and Tian M 2019 *Chin. Phys. B* **28** 087503
[9] Jiang W, Chen G, Liu K, Zang J, te Velthuis S G E and Hoffmann A 2017 *Phys. Rep.* **704** 1
[10] Liu Y H and Li Y Q 2015 *Chin. Phys. B* **24** 017506
[11] Tang J, Wu Y, Kong L, Wang W, Chen Y, Wang Y, Soh Y, Xiong Y, Tian M and Du H 2021 *Natl. Sci. Rev.* **8** nwaa200
[12] Ogawa N, Koshibae W, Beekman A J, Nagaosa N, Kubota M, Kawasaki M and Tokura Y 2015 *Proc. Natl. Acad. Sci. USA* **112** 8977
[13] Jiang W, Upadhyaya P, Zhang W, Yu G, Jungfleisch M B, Fradin F Y, Pearson J E, Tserkovnyak Y, Wang K L, Heinonen O, te Velthuis S G E and Hoffmann A 2015 *Science* **349** 283
[14] Peng L C, Zhang Y, Zuo S L, He M, Cai J W, Wang S G, Wei H X, Li J Q, Zhao T Y and Shen B G 2018 *Chin. Phys. B* **27** 066802
[15] Grundy P J and Herd S R 1973 *Phys. Stat. Sol. (a)* **20** 295
[16] Nagaosa N and Tokura Y 2013 *Nat. Nanotechnol.* **8** 899
[17] Zhang C L, Wang J N, Song C K, Mehmood N, Zeng Z Z, Ma Y X, Wang J B and Liu Q F 2022 *Rare Met.* **41** 865
[18] Mehmood N, Wang J, Zhang C, Zeng Z, Wang J and Liu Q 2022 *J. Magn. Magn. Mater.* **545** 168775
[19] Cui B, Yu D, Shao Z, Liu Y, Wu H, Nan P, Zhu Z, Wu C, Guo T, Chen P, Zhou H A, Xi L, Jiang W, Wang H, Liang S, Du H, Wang K L, Wang W, Wu K, Han X, Zhang G, Yang H and Yu G 2021 *Adv. Mater.* **33** 2006924
[20] Jena J, Göbel B, Ma T, Kumar V, Saha R, Mertig I, Felser C and Parkin S S P 2020 *Nat. Commun.* **11** 1115
[21] Peng L, Takagi R, Koshibae W, Shibata K, Nakajima K, Arima T H, Nagaosa N, Seki S, Yu X and Tokura Y 2020 *Nat. Nanotechnol.* **15** 181
[22] Khanh N D, Nakajima T, Yu X, Gao S, Shibata K, Hirschberger M, Yamasaki Y, Sagayama H, Nakao H, Peng L, Nakajima K, Takagi R, Arima T H, Tokura Y and Seki S 2020 *Nat. Nanotechnol.* **15** 444
[23] Šimšová J, Tomáš I, Görnert P, Nevřiva M and Maryško M 1979 *Phys. Status Solidi A* **53** 297
[24] Bonner W A, LeCraw R C, Pierce R D and Van Uitert L G 1978 *J. Appl. Phys.* **49** 1871
[25] Shao Q, Liu Y, Yu G, Kim S K, Che X, Tang C, He Q L, Tserkovnyak Y, Shi J and Wang K L 2019 *Nat. Electron.* **2** 182
[26] Ding S, Ross A, Lebrun R, Becker S, Lee K, Boventer I, Das S, Kurokawa Y, Gupta S, Yang J, Jakob G and Kläui M 2019 *Phys. Rev. B* **100** 100406
[27] Büttner F, Mawass M A, Bauer J, Rosenberg E, Caretta L, Avci C O, Gräfe J, Finizio S, Vaz C A F, Novakovic N, Weigand M, Litzius K, Förster J, Träger N, Groß F, Suzuki D, Huang M, Bartell J, Kronast F, Raabe J, Schütz G, Ross C A and Beach G S D 2020 *Phys. Rev. Mater.* **4** 011401
[28] Vélez S, Ruiz-Gómez S, Schaab J, Gradauskaite E, Wörnle M S, Welter P, Jacot B J, Degen C L, Trassin M, Fiebig M and Gambardella P 2022 *Nat. Nanotechnol.* **17** 834
[29] Liu Q B, Meng K K, Xu Z D, Zhu T, Xu X G, Miao J and Jiang Y 2020 *Phys. Rev. B* **101** 174431
[30] Yang Y, Liu T, Bi L and Deng L 2021 *J. Alloys Compd.* **860** 158235
[31] Tan S, Liu Y, Chen J, Yang L, Lan J and Dai B 2019 *Journal of Materials Science: Materials in Electronics* **30** 7410
[32] Kim Y, Bang D J, Kim Y and Kim K H 2020 *AIP Adv.* **10** 025306
[33] Mattheis R and Quednau G 1999 *J. Magn. Magn. Mater.* **205** 143
[34] Ma S, Tan A, Deng J X, Li J, Zhang Z D, Hwang C and Qiu Z Q 2015 *Sci. Rep.* **5** 11055
[35] Chen G, Li J, Liu F Z, Zhu J, He Y, Wu J, Qiu Z Q and Wu Y Z 2010 *J. Appl. Phys.* **108** 073905
[36] Shi Z, Jiang H Y, Zhou S M, Hou Y L, Ye Q L and Su Si M 2016 *AIP Adv.* **6** 015101
[37] Qiao S, Nie S, Zhao J and Zhang X 2015 *J. Appl. Phys.* **117** 093904
[38] Boudiar T, Payet-Gervy B, Blanc-Mignon M F, Rousseau J J, Le Berre M and Joisten H 2004 *J. Magn. Magn. Mater.* **284** 77
[39] Hirai Y, Yoshikawa N, Hirose H, Kawaguchi M, Hayashi M and Shimano R 2020 *Phys. Rev. Appl.* **14** 064015
[40] Caretta L, Rosenberg E, Büttner F, Fakhrul T, Gargiani P, Valvidares M, Chen Z, Reddy P, Muller D A, Ross C A and Beach G S D 2020 *Nat. Commun.* **11** 1090
[41] Nahid M A I and Suzuki T 2004 *J. Magn. Magn. Mater.* **282** 260